PROCEEDINGS, 51st Workshop on Geothermal Reservoir Engineering
Stanford University, Stanford, California, February 9-11, 2026
SGP-TR-230

# Design and Implementation of a New Multi-frac Stimulation Concept in Utah FORGE EGS

[1]Ruwantha Ratnayake, [1]Ahmad Ghassemi, [2]Robert Jeffrey

[1]University of Oklahoma, Oklahoma

[2]SCT Operations

ahmad.ghassemi@ou.edu; rruwantha13@ou.edu

**Keywords:** Stimulation, hydraulic fracturing, EGS, FORGE, shear slip

## ABSTRACT

Multistage hydraulic fracturing in horizontal wells is a commonly used technique to enhance the permeability of unconventional reservoirs and enhanced geothermal systems (EGS). The U.S. Department of Energy's FORGE (Frontier Observatory for Geothermal Energy) initiative is an EGS field laboratory in which multistage hydraulic fracturing is applied in horizontal wells with the objective of improving connectivity between injection and production wells. Several fracturing stages have already been carried out with satisfactory results. This paper presents a design and implementation of a new multi fracture stimulation concept for Utah FORGE. In the first section, a new stimulation stage is proposed in well 16A(78)-32 above the previously fractured Stage 9, at a measured depth (MD) of 8950ft. The stage includes three closely spaced clusters (3.5 m spacing), stimulated sequentially for 70, 80, and 90 minutes, respectively. The simulated fractures are oval-shaped and propagate primarily toward well 16B(78)-32, attributed to the prevailing stress gradient. Because of the tight spacing, significant shear deformation develops near the injection point and at the leading edges of the fractures. This shear deformation is expected to increase fracture conductivity and promote wing-crack development, thereby improving fracture connectivity. Next, a sensitivity analysis is performed by circulating cold water through a three-fracture cluster to identify an optimal cluster spacing. Results indicate that thermal performance improves as fracture spacing increases; however, the injectivity index increases up to a spacing of 4 m and then decreases at 6 m. These findings highlight the need to balance thermal performance with injectivity when selecting the cluster spacing for the proposed stimulation design.

## 1. INTRODUCTION

The Utah FORGE project relies on multistage fracturing along its highly deviated wellbores, proving a testbed for different schemes to achieve sustainable reservoir permeability. Currently, well 16A(78)-32 which was completed in 2020 serves as the injection well and well 16B(78)-32 (located nominally 300ft above the injection well) which was completed in July 2023 is the production well (Xing et al., 2024). The injection well was stimulated in April of 2022 using three stages (1-3) where Stage 1 was an open hole and Stages 2 and 3 were cased and cemented with a single perforated interval (Moore et al., 2023; Lee et al., 2022; Lee & Ghassemi, 2023). The main objective of this work is to design and implement a new reservoir stimulation concept in Utah FORGE with an emphasis on improving fracture-wellbore connectivity while enhancing simulated reservoir volume (SRV) and heat exchange efficiency by enhancing fracture self-propping. To achieve this objective, it is proposed to create multiple (three to five, depending on cost and budget constraints) narrow SRV zones with three to five closely spaced hydraulic fractures that are generated sequentially. one key advantage of the proposed approach is that the close spacing of the fractures induces strong pressure and stress changes on the adjacent rock, thereby promoting shear slip, the formation of wing cracks, and the activation and opening of adjacent hydraulic fracturs as well as inducing stress change on small pre-existing natural fractures. In addition, these zones are expected to experience strong thermo-poroelastic stress during stimulation and production, leading to further deformation on existing natural fractures, promoting cross-flow between the main hydraulic fractures. Simulations are used to assess placing closely spaced hydraulic fractures, and to study the expected heat production potential.

## 2. SET UP AND IMPLEMENTATION OF NEW PROPOSED STAGE

We intend to target a zone within the well 16A above Stage 10 that is expected to have few or no natural fractures. The FMI log indicates zones 8885-8860 ft and 8778-8740 ft and 8600-8550 ft (MD) meet this criterion. In selecting this zone we are considering the location of previous frac hits in 16B from frac Stages 8-10, to avoid interference during stimulation and circulation. Currently, we expect to use an injection rate of 10-15 bbl/min in each frac stage. So the new proposed Stage is set at a MD of 8950ft such that the distance between the last cluster on Stage 9 and the first cluster of proposed Stage is approximately 250ft. The proposed stage consists of three clusters with a cluster spacing of 3 to 3.5m. Figure 1 shows the positions of all Stages along with the newly proposed Stage in 16A. Currently the plan calls for use of abrasive jet perforating instead of explosive perforations.

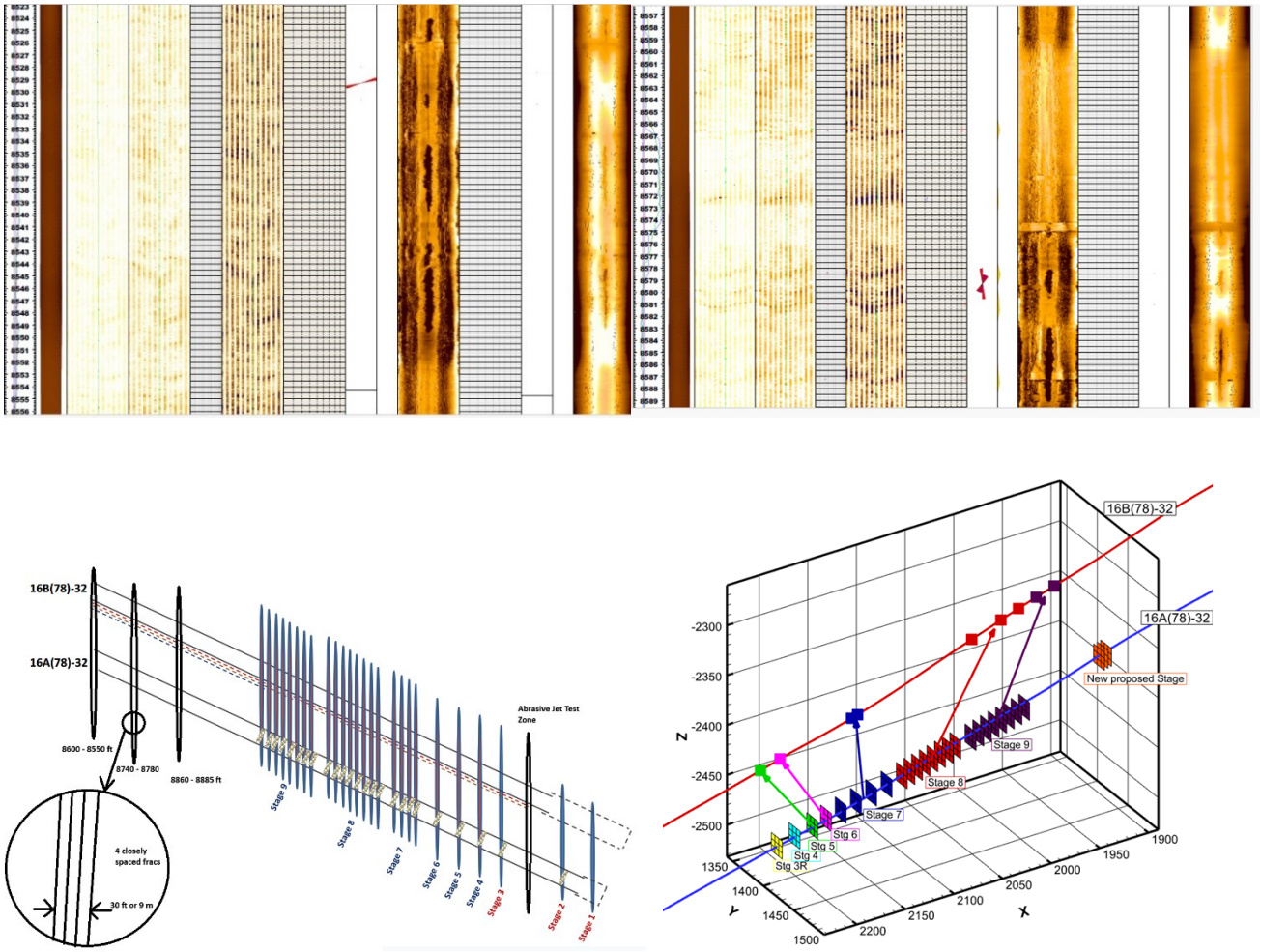


**Figure 1: (top): FMI log of 8600-8525 ft (MD), 8885-8860 ft and 8778-8740 ft do not show many natural fractures (not all images are shown). (bottom): Stage and fracture driven interaction locations.**

The injection rates and location suitability with respect to fracture driven interactions (FDI) are analyzed based on a series of forward numerical simulations. The modeling is based on the 3D displacement discontinuity method coupled with the finite element method for flow within the fractures. The formation properties that were used in this study are summarized in Table 1. The injection rate for this case was set to 11.7 bpm, based on rates used in prior Utah FORGE stimulations and published literature. In the field, Stage 9 was pumped at approximately 80 bpm across 8 clusters, corresponding to about 10 bpm per cluster; therefore, a three-cluster stage would scale to a total rate of roughly 30 bpm. However, Kumar and Ghassemi (2023) indicate that a substantial fraction of the injected fluid can be lost to leakoff (≈ 60%), meaning only about 40% contributes to fracture inflation and propagation. Applying this leakoff correction results in the 11.7 bpm injection rate adopted in this study.

**Table 1: Input data for the simulation (Ye & Ghassemi, 2024).**

| | | | |
|---|---|---|---|
| G | Shear Modulus | $2.088 \times 10^4$ | MPa |
| ν | Poisson's ratio | 0.29 | - |
| k | Permeability | $9.0 \times 10^{-16}$ | $m^2$ |
| φ | Porosity | 5.0 | % |
| $\mu_l$ | Fluid viscosity slickwater | $0.24 \times 10^{-3}$ | Pa.s |
| ρ | Density slickwater | 966.97 | $kg/m^3$ |
| $S_h$ | Minimum horizontal stress gradient | 0.01651 (0.73) | MPa/m (psi/ft) |
| $S_H$ | Maximum horizontal stress gradient | 0.02182 (1.03) | MPa/m (psi/ft) |
| $S_V$ | Vertical stress gradient | 0.02556 (1.13) | MPa/m (psi/ft) |

| | | | |
|---|---|---|---|
| pp | Pore pressure gradient | 0.00979 (0.433) | MPa/m (psi/ft) |
| $KI_c$ | Mode I fracture toughness | $2.6 \times 10^6$ | $Pa.m^{0.5}$ |
| - | Perforation diameter | 0.015 | m |
| - | Discharge coefficient of perforations | 0.75 | - |
| Q | Injection rate for the stimulation | 11.7 | bpm |
| - | Minimum (residual) aperture | 0.1 | mm |
| - | Normal stiffness ($K_n$) | $1 \times 10^{10}$ | Pa/m |
| - | Shear stiffness ($K_s$) | $1 \times 10^{10}$ | Pa/m |

The plan is to fracture the deepest cluster first, followed by sequential stimulation of the overlying clusters moving up the well. The injection is conducted such that cluster 1 is stimulated for 70 minutes, cluster 2 for 80 minutes and cluster 3 for 90 minutes. The time of stimulation duration was progressively increased for successive clusters to overcome the stress shadow effects created by the previously created fractures, which are amplified due to the close cluster spacing. Figure 2 shows the final shapes of the resulting HF geometries at 70,150 and 240 minutes (see also Figure 5).

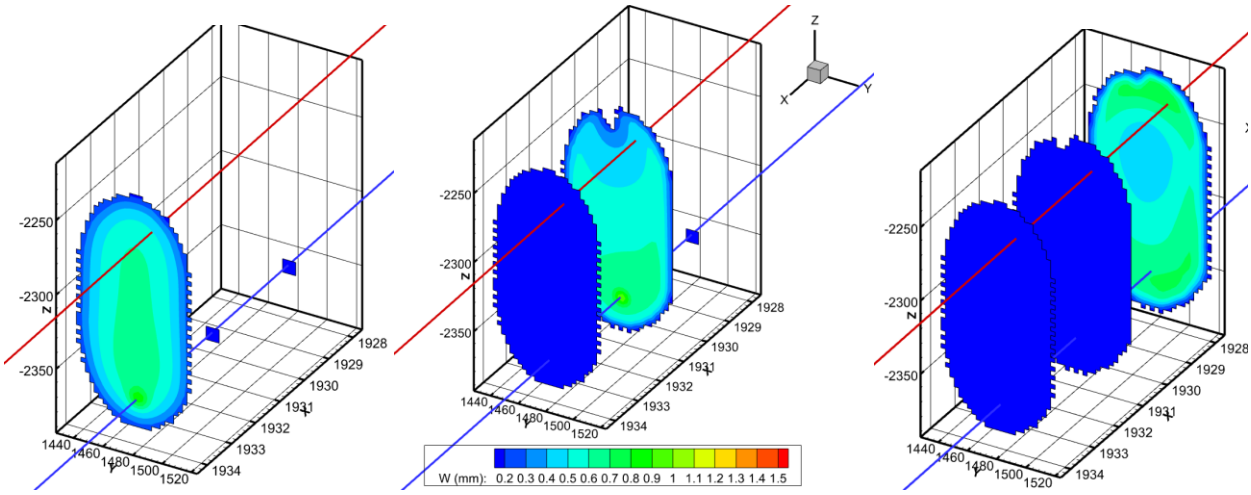


**Figure 2: Simulation of a new stage above Stage 10 in Utah FORGE at a measured depth (well 16A) of 8950ft. The cluster spacing is 3.5m. Pumping for 70 minutes, 80 minutes, and 90 minutes for each cluster using a constant injection rate of 11.7 bbl/min.**

As shown in the figure, all three clusters generated oval shaped hydraulic fractures with propagation primarily in the positive z-direction due to the prevailing Shmin stress gradient. The fractures produced by all three clusters are of comparable size, with an average width of approximately 80 m and a height of about 140 m. The maximum fracture aperture reaches approximately 1.2 mm in the vicinity of the injection point. It is also observed that fractures created earlier (see fracture 1 and 2 in Figure 2) tend to close as subsequent fractures propagate, due to the stress shadow effects induced by newly formed fractures.

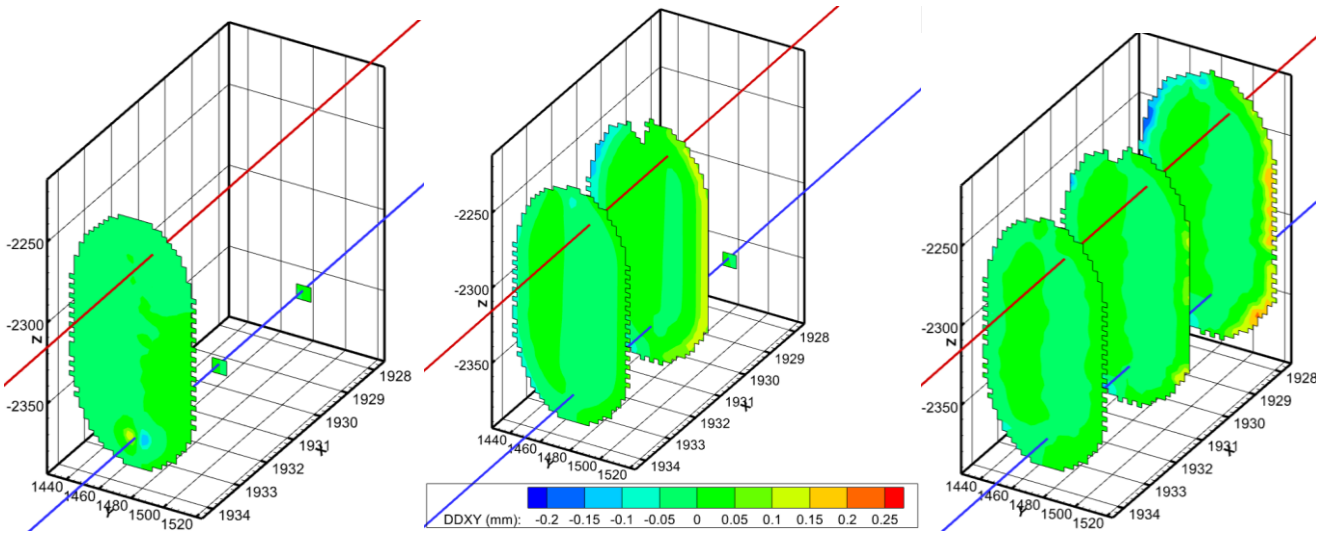


**Figure 3: Distribution of shear deformation in y-direction at 70, 150 and 240 minutes past injection.**

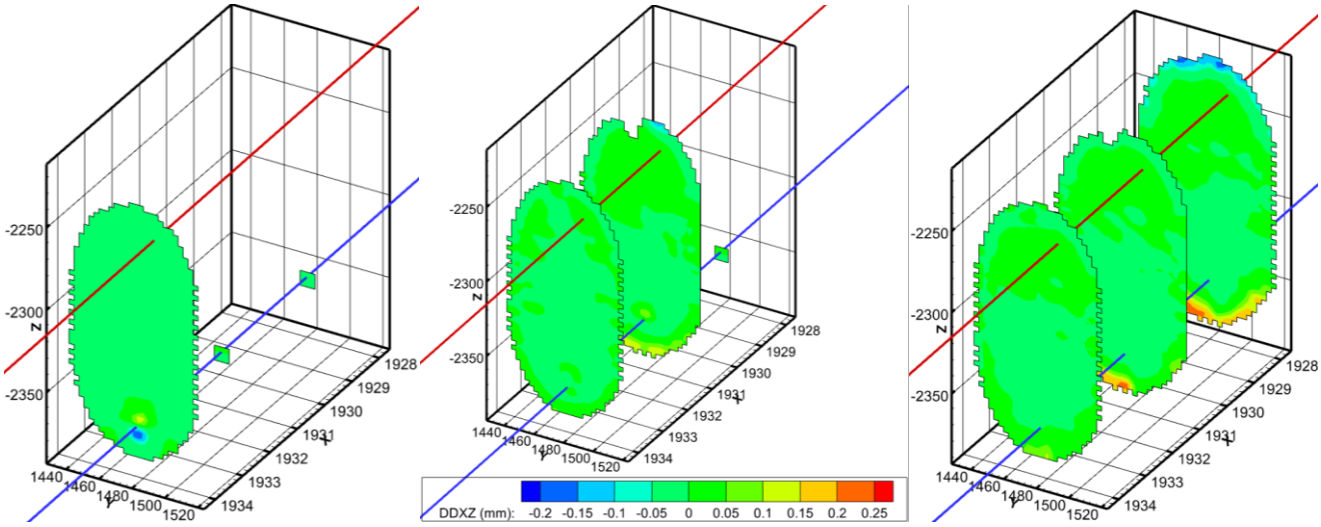


**Figure 4: Distribution of shear deformation in z-direction at 70, 150 and 240 minutes past injection.**

Figure 3 and Figure 4 show the distribution of shear deformation in the fractures in y- and z-directions during different stages of the stimulation. In both directions, the maximum shear deformation reaches approximately 0.25mm and is primarily concentrated near the fracture tips and around the injection point. This shear behavior is mainly attributed to the small fracture spacing. When fractures are closely spaced, the propagation of one fracture generates strong stress shadow effects that locally rotate the principal stress directions in the vicinity of adjacent fractures. This localized stress rotation induces shear deformation on the fracture surfaces. Additionally, the high shear at the fracture tips results in wing cracks increasing the fracture surface area. This intentional shearing is beneficial as it enhances fracture permeability via dilation and self-propping and improves fluid circulation and heat extraction efficiency (see Ghassemi et al., 2026). The above simulations show that using the proposed injection rates, sufficient fracture growth can be achieved to intersect the production wellbore. However, the rates may need to be increased to 15bbl/min if natural features appear on the path of fracture growth. Next, the injectivity and heat extraction potential from such a cluster of fracture will be studied.

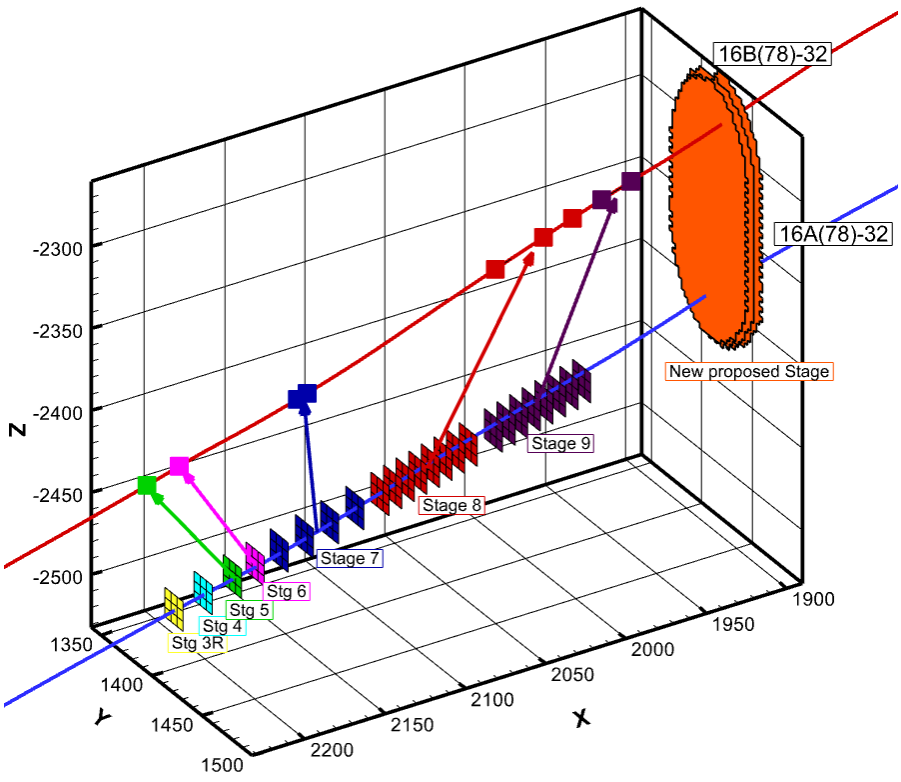


**Figure 5: Locations of Stages 3R–9 and the newly proposed stage in well 16A, along with the corresponding frac-hit location in well 16B.**

### 3. INJECVITY, HEAT EXTRATION POTENTIAL AND THE IMPACT OF CLUSTER SPACING

A major aspect of the proposed stimulation design is to attain high injectivity and heat extraction potential. The near well pressure losses and the amount of heat energy produced is highly dependent on the well layout and geometry of the fracture network. Cluster spacing is a key parameter in designing the fracturing plan for an EGS. If the spacing is too small, the region affected by major fractures may overlap, reducing the fracturing efficiency. Conversely, if the spacing is too large, the area between the fractures may not contribute to production, thereby lowering overall efficiency.

It is widely understood that tighter cluster spacing can increase energy production, as a denser fracture network promotes superior fluid flow and greater fluid rock interaction within the formation. Furthermore, closely spaced clusters may amplify stress shadow effects, which can limit fracture propagation and reduce production from these clusters (Gringarten et al., 1975). Therefore, determining the optimal cluster spacing, number of clusters, and hydraulic fracture geometry is critical when planning reservoir stimulation. A closely spaced fracture system is expected to act, during heat production, like individual fractures in the short time and like a single fracture in the long time.

This section examines the effects of fracture geometry and spacing on heat production in Utah FORGE EGS. The first three cases considered are based on cluster design where three fractures (perfs) are placed at 1m, 2m, 4m and 6m intervals, respectively. In the fourth case, a stage with a single fracture is considered for comparison. Formation properties and in-situ stresses specific to Utah FORGE, as listed in Table 1 and Table 2, are used as the basis for this analysis. Simulations are performed using a fully coupled thermoporoelastic fracture model, in which fracture apertures are allowed to evolve in response to the thermoporoelastic stresses that develop during circulation.

It should be noted that although the hydraulic fracture stimulation modeling in the previous section resulted in three oval-shaped fractures with dimensions of approximately 140 m × 80 m, the fracture geometry and size were reduced in the present analysis due to computational limitations. In this section rectangular fractures with dimensions 25 m × 15 m were used. Accordingly, the fluid circulation rates were scaled down to reflect the reduced fracture size. All cases were carried out assuming a minimum production of 1 bbl/min per well. Considering 10 stages in the well, the fluid injection rate was set at 0.113 bbl/min per cluster, with an extraction pressure of 27 MPa. The circulation was carried out for a period of 140 days.

**Table 2: In situ stress and formation properties (Ye & Ghassemi, 2024).**

| Parameter | Value | Units |
|---|---|---|
| Rock permeability | $1.20\times10^{-17}$ | $m^2$ |
| Biot's coefficient ($\alpha$) | 0.50 | - |
| Undrained Poisson's ratio | 0.32 | - |
| Rock density($\rho_R$) | 2650 | $kg/m^3$ |
| Fluid heat capacity ($C_F$) | 4200 | J/kg.K |
| Rock heat capacity ($C_R$) | 800 | J/kg.K |
| Rock thermal conductivity ($K_R$) | 2.9 | - |
| Rock linear thermal expansion coefficient ($\alpha_T$) | $6.6\times10^{-7}$ | - |
| Injection of fluid temperature ($T_i$) | 353 | K |
| Initial rock temperature ($T_0$) | 448 | K |
| In-situ stress vertical | 65.13 | MPa |
| In-situ stress maximum horizontal | 55.88 | MPa |
| In-situ stress minimum horizontal | 45.81 | MPa |

The first case involves three rectangular, parallel fractures with dimensions of 25 m × 15 m, placed at a spacing of 1 m. **Figure 6**(a) shows the resulting temperature distribution inside the fractures over time. As shown, the temperatures in the two exterior fractures are distributed similarly, while the fracture in the middle has undergone more cooling. By the end of the 140-day circulation period, the fracture area in the vicinity of the injection well in all three fractures has cooled down to the injection temperature with the fracture in middle exhibiting a comparatively larger cooled region.

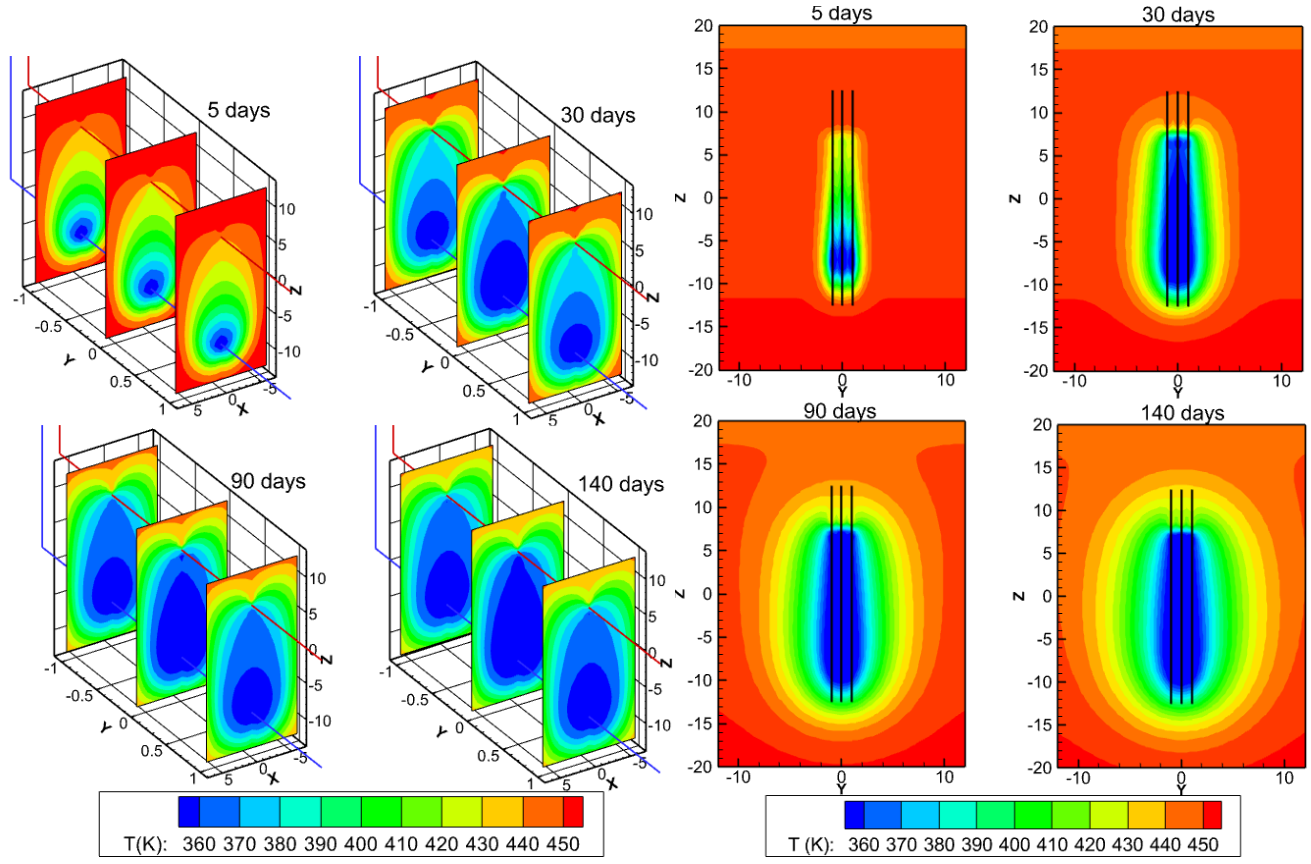


**Figure 6: Temperature distribution (a) inside the fractures; (b) in a cross section of the XY plane around the fractures, when the cluster spacing is 1m.**

**Figure 6**(b) illustrates the temperature distribution in a cross section of the ZY plane around the fractures. Black lines in the cross section represents the 3 fractures. As shown, after 140 days of circulation, the rock matrix in the immediate vicinity of the fractures has almost cooled down to the injection temperature, extending up to approximately 2 m from the fracture surfaces. Based on this cross section in **Figure 6**(b) it can be inferred that the two outer fractures have some potential to produce for even longer as they are exposed to the open rock matrix on one side. In contrast, the middle fracture is expected to show a rapid decline in production temperature, since it is bounded by two outer fractures and the volume in between them has already cooled. This effect arises because the surrounding rock matrix is simultaneously cooled from both sides, as also reflected in the temperature trends shown in **Figure 6**(a). Any crossflow between fractures is ignored in this simulation. Such crossflow would tend to result in more uniformity between fracture cooling. To evaluate how increasing fracture spacing influences this behavior, the next two cases are analyzed.

**Figure 7**(a), (b) illustrate the temperature distribution within the fractures and the rock matrix respectively when the fracture spacing is increased to 2 m. Compared to the results for a 1m spacing, the temperature distributions show minimal change. However, in the later stages of circulation, the temperature of the rock matrix between the fractures reaches the injection temperature, as evident in **Figure 7**(b).

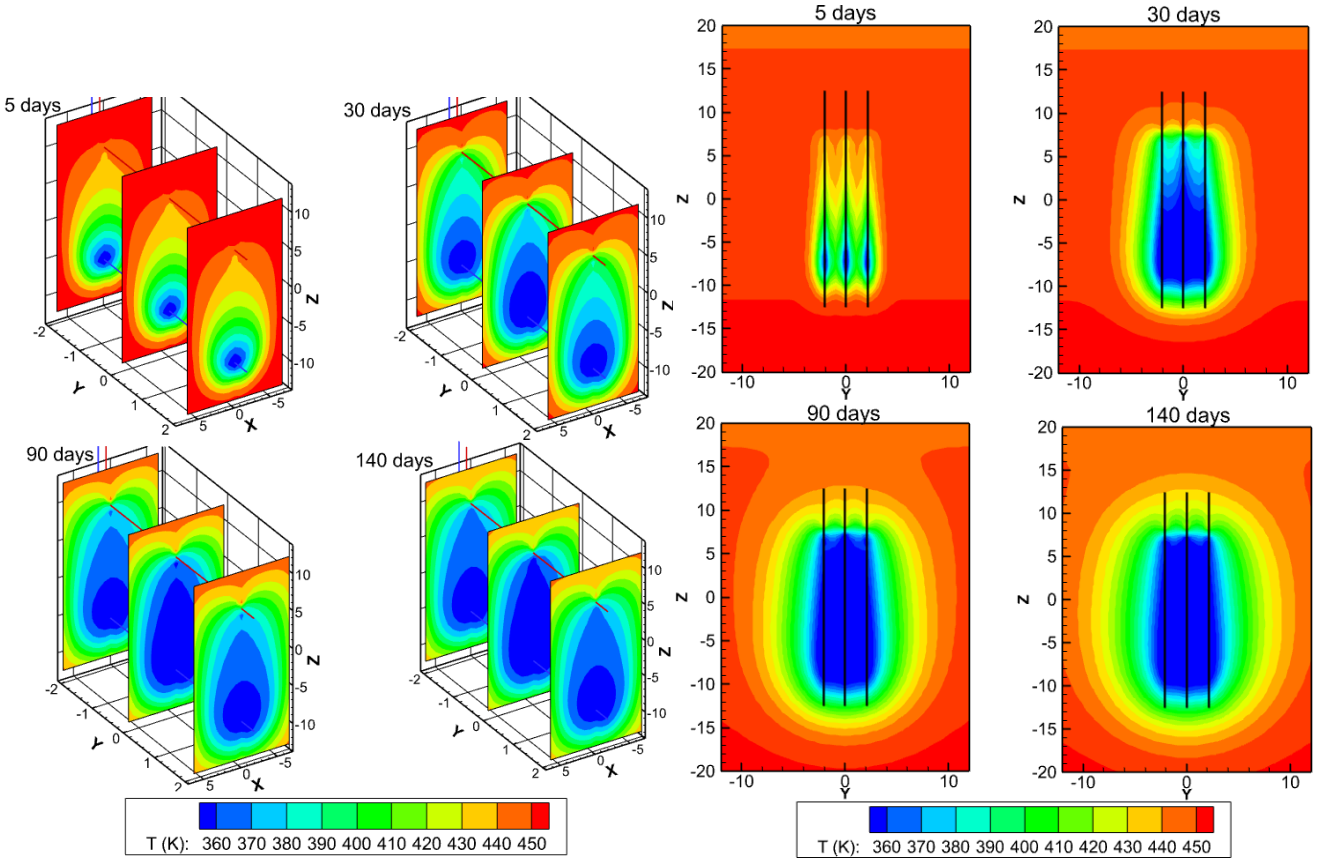


**Figure 7: Temperature distribution (a) inside the fractures; (b) in a cross section of the XY plane around the fractures, when the cluster spacing is 2m.**

The next case considered maintains the same fracture geometry and boundary conditions as the previous case, but the cluster spacing is increased to 4 m. **Figure 8**(a) illustrates the temperature distribution within the fractures at various times during fluid circulation.

When comparing the temperature distribution plots for the 1 m and 2 m cluster spacing cases, it becomes evident that with a 4 m cluster spacing, it takes significantly longer for the fracture to cool down to the injection temperature. This observation is further supported by the production temperature versus time plots, which are discussed in the next section.

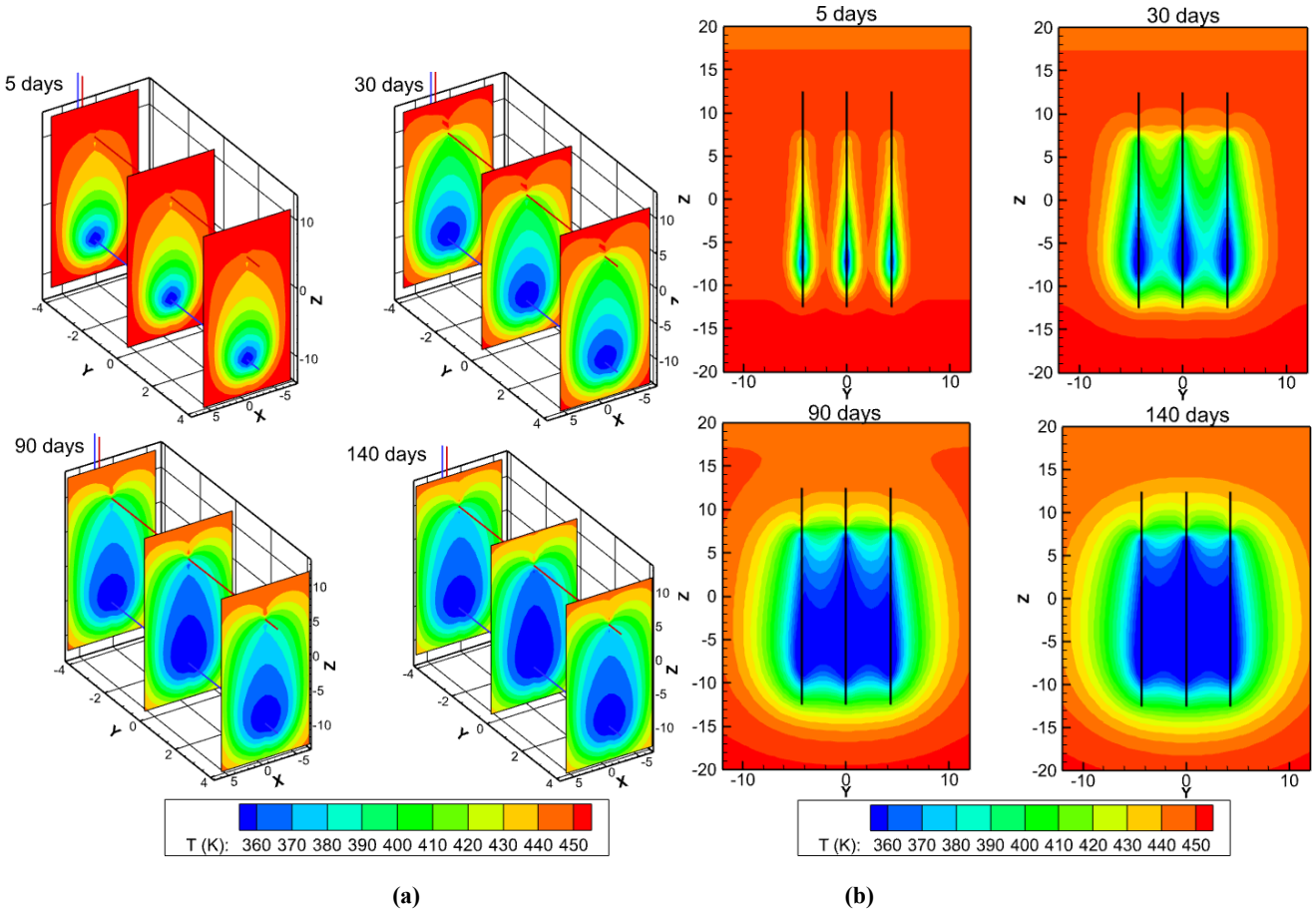


**Figure 8: Temperature distribution (a) inside the fractures; (b) in a cross section of the XY plane around the fractures, when the cluster spacing is 4m.**

**Figure 8**(b) shows the temperature distribution in a cross section of the YZ plane around the fractures when the cluster spacing is 4m. When comparing this plot to the 2m spacing case in **Figure 7**(b), the primary difference lies in the temperature distribution in the rock matrix between the fractures rather than in the rock matrix on the outer sides of the fractures. In between the fractures, the rock matrix in 2m spacing case has undergone more cooling than the 4m spacing case. This difference is primarily due to the increased exposure of the rock matrix to the central fracture as a result of increased fracture spacing. The impact of this increased spacing on production temperature will be discussed in the next section.

The next geometry considered was a single rectangular fracture with the same dimensions as in the previous cases. Fluid circulation was maintained with an injection rate of 0.113 bbl/min and an extraction pressure of 27 MPa to be consistent with the previous case. The results (see **Figure 9**(a), (b)) indicate that the cooling of the fracture is significantly faster compared to the previous cases with three parallel fractures. This faster cooling can primarily be attributed to the reduced number of fractures, which increases the cooling rate (since the total injection rate is the same), which eventually makes the overall cooling of the reservoir matrix faster.

This observation is further validated with the cross-sectional temperature distribution plots shown in **Figure 9**(b). Compared to the previous two cases, the temperature in the immediate vicinity of the fracture shows a high decline. However, there is no significant difference in the temperature of the far field rock matrix. These results confirm that for this reservoir, using stages with multiple closely spaced clusters is more effective than using single cluster stages.

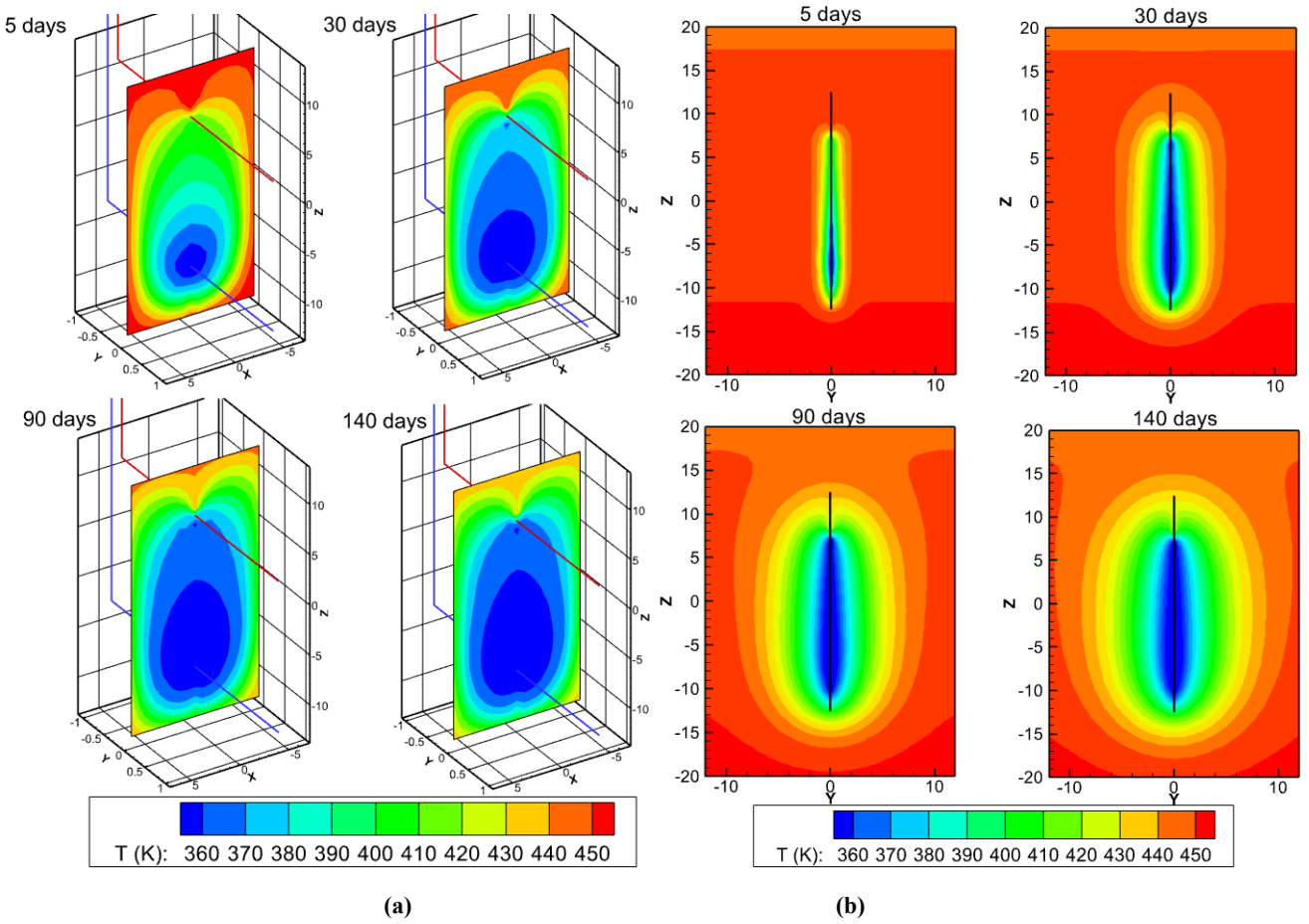


**Figure 9: Temperature distribution (a) inside the fracture; (b) in a cross section of the XY plane around the fractures, for the single fracture case.**

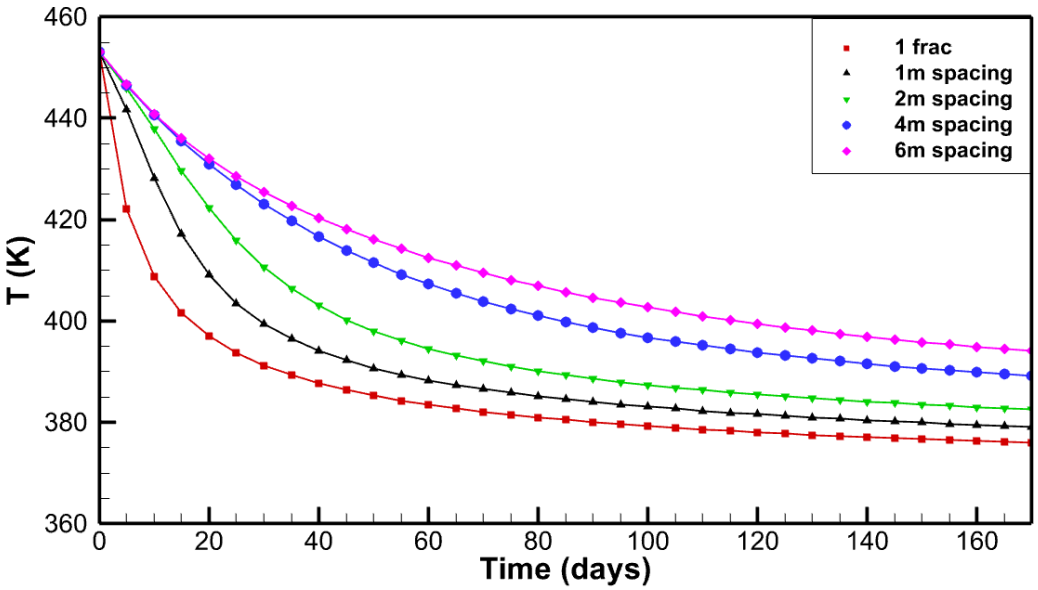


**Figure 10: Production temperature vs time plots for all cases considered.**

**Figure 10** illustrates the production temperature versus time plots for all the cases previously considered. As shown in the plot, the 6m spacing case maintains the highest production temperature over time, while the single fracture case exhibits the lowest. Interestingly, as discussed in the previous section, the production temperature increases when the cluster spacing is increased from 1m to 2m to 4m. The relatively slow decline in production temperature with increasing fracture spacing occurs because of the increased rock matrix between fractures. As a result, the central fracture experiences less rapid cooling compared to cases where fractures are positioned closer together.

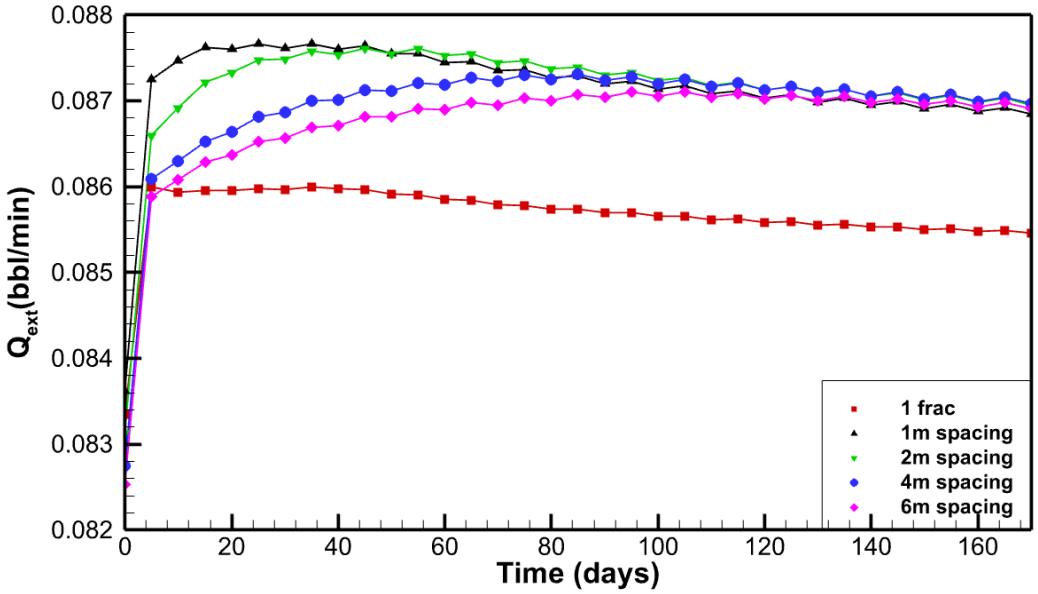


**Figure 11: Production rate vs time plots for all cases considered.**

However, interpreting these results requires considering the total production rates in each scenario, as power generation depends on both production temperature and production rate. **Figure 11** presents the variation in production rates across all cases. Notably, the single-fracture case exhibits a significantly lower production rate despite identical injection rates across all cases. This occurs because a single fracture experiences a higher leak-off rate. In contrast, when multiple fractures are closely spaced, the leak-off rate decreases due to increased pressure in the rock matrix and the effect of fracture dilation. Consequently, the highest production rate is observed in the case with the smallest fracture spacing (see **Figure 11**).

It should also be noted that when spacing is close (1 m, 2 m), the production rate trends downward as circulation continues, whereas this is not evident at larger spacing. A likely reason is stress shadowing from neighboring clusters, which limits fracture dilation; as dilation is reduced, the production rate continues to drop. At larger spacing, the stress shadow is weaker, so this effect is minimal.

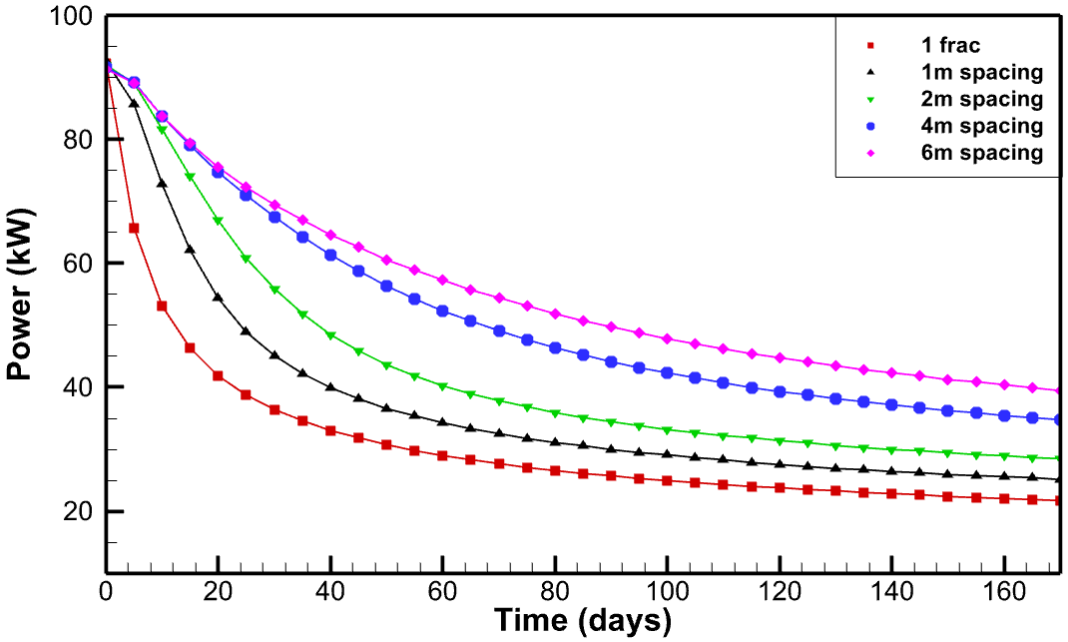


**Figure 12: Power generated vs time plots for all cases considered.**

**Figure 12** illustrates the change in power generated with time for each case considered. Power generation accounts for both production temperature and production rate, making it a suitable parameter for comparing the different fracture spacing scenarios. An efficiency of 100% was assumed when calculating power in Figure 12. The results show that the power generation increases with increasing fracture spacing, primarily due to exposure of larger rock volume for heat extraction as spacing increases. However, this increase is not gradual. The largest gain in power output occurs when spacing increases from 2 m to 4 m, whereas a further increase to 6 m results in only a

marginal improvement. This behavior indicates that beyond a certain spacing, increasing fracture separation no longer contributes significantly to power production.

This limiting spacing can be estimated by examining the temperature distribution in the cross-section of the single-fracture case shown in Figure 9(b). At 140 days, the cooling front has propagated more than 12 m into the surrounding rock matrix. For parallel fractures, this distance is effectively doubled because cooling fronts advance from both fractures. Therefore, for the reservoir properties considered in this study, the fracture spacing beyond which power production no longer increases can be estimated to be approximately 24 m.

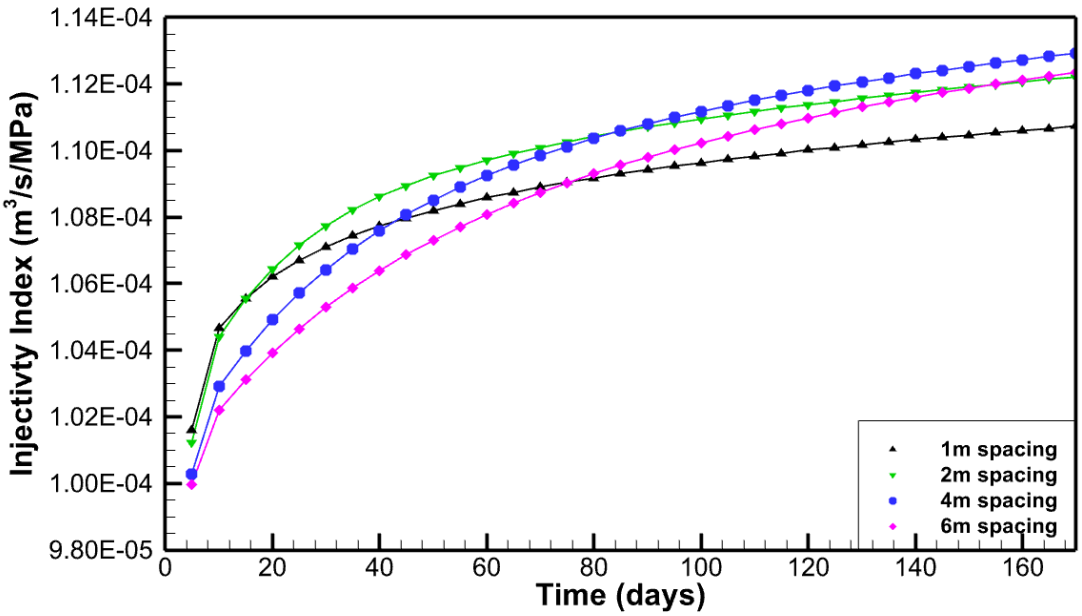


**Figure 13: Injectivity Index vs time plots for all cases considered.**

The injectivity results were also calculated and plotted for the cases considered and are presented in Figure 13. For all spacings, injectivity increases gradually with time, indicating progressive improvement in the ability of the fracture system to accept fluid. It can be noticed that cluster spacing has a smaller, yet noticeable effect on injectivity index. The tightest spacing (1m) results in the lowest long-term injectivity, which is attributed to strong stress shadow effect that increases the pressure inside the fracture. Overall 4m spacing maintains the highest injectivity over the simulation period. These trends indicate that spacing selection should consider both thermal performance and hydraulic performance. While power production increases with spacing and is highest for the 6 m case, injectivity reaches a maximum at 4 m and decreases slightly at 6 m, highlighting the need to balance thermal performance against injectivity.

## 4. CONCLUSIONS

This study developed and evaluated a new multi fracture stimulation setup for Utah FORGE aimed at improving connectivity between wells 16A(78)-32 and 16B(78)-32. The new stage placed at 8,950 ft MD above Stage 9, with three closely spaced clusters (3.5 m) stimulated sequentially, produced oval-shaped fractures that mainly propagated toward the production well. The tight spacing also created noticeable shear deformation near the injection point and at the fracture tips, which is likely to increase fracture conductivity and encourage wing crack growth, thereby improving connectivity, crossflow, and potential SRV formation. A subsequent sensitivity study showed that wider fracture spacing improves thermal performance because of larger effective rock volume; however, the injectivity index increases up to a spacing of 4 m and then decreases at 6 m, indicating that spacing selection must balance between thermal and hydraulic performance. The heat extraction scenarios did not consider the influence of any crossflows and so additional analysis is needed. Overall, the results support the proposed multi fracture approach for Utah FORGE and suggest that moderate spacing is likely the best balance between power generation and injectivity.

## ACKNOWLEDGEMENT

This project was supported by the Utah FORGE project sponsored by the U.S. Department of Energy, through the project “Design and Implementation of a Novel Multi-frac Stimulation Concept in Utah FORGE.”

**REFERENCES**

Gringarten, A. C., Witherspoon, P. A., & Ohnishi, Y. (1975). Theory of heat extraction from fractured hot dry rock. Journal of Geophysical Research, 80(8), 1120–1124. https://doi.org/10.1029/JB080i008p01120

Kumar, D., & Ghassemi, A. (2023), Hydraulic Fracturing in Petroleum and Geothermal Reservoirs with Reference to the Utah FORGE Stimulation, 48 th Workshop on Geothermal Reservoir Engineering.

Lee, S. H., & Ghassemi, A. (2023). Modeling and Analysis of Stimulation and Fluid Flow in the Utah FORGE Reservoir. 48th Workshop on Geothermal Reservoir Engineering.

Lee, S. H., Ratnayake, R., & Ghassemi, A. (2022). Numerical Analysis of Fluid Stimulation in Fractured Utah FORGE Wells. Geothermal Rising Conference, 46.

Moore, J., McLennan, J., Pankow, K., Finnila, A., Dyer, B., Karvounis, D., Bethmann, F., Podgorney, R., Rutledge, J., Meir, P., Xing, P., Jones, C., Barker, B., Simmons, S., & Damjanac, B. (2023, June 28). Current Activities at the Utah Frontier Observatory for Research in Geothermal Energy (FORGE): A Laboratory for Characterizing, Creating and Sustaining Enhanced Geothermal Systems. ARMA US Rock Mechanics/Geomechanics Symposium.

Xing, P., England, K., Moore, J., Podgorney, R., & McLennan, J. (2024). Analysis of Circulation Tests and Well Connections at Utah FORGE. 49th Workshop on Geothermal Reservoir Engineering.

Ye, Z., & Ghassemi, A. (2024). The Updated Wellbore Stress Models for Utah FORGE. 49th Workshop on Geothermal Reservoir Engineering.